

# Symmetry-protected non-Abelian geometric phases in optical waveguides with nonorthogonal modes

Julien Pinske and Stefan Scheel\*

*Institut für Physik, Universität Rostock, Albert-Einstein-Straße 23-24, D-18059 Rostock, Germany*

(Dated: January 8, 2022)

The generation of non-Abelian geometric phases from a system of evanescently coupled waveguides is extended towards the framework of nonorthogonal coupled-mode theory. Here, we study an experimentally feasible tripod arrangement of waveguides that contain dark states from which a nontrivial  $U(2)$ -mixing can be obtained by means of an adiabatic parameter variation. We investigate the influence of higher-order contributions beyond nearest-neighbour coupling as well as self-coupling on the stability of a  $U(3)$ -phase generated from an optical tetrapod setup. Our results indicate that, despite the mode nonorthogonality, the symmetry of dark states protects the geometric evolution of light from distortion.

## I. INTRODUCTION

Abelian as well as non-Abelian gauge theories feature prominently in modern theories of fundamental interactions. They also occur frequently in a variety of geometric settings and are therefore central to much of modern mathematics. Their formulation in terms of gauge fields is deeply connected to the notion of a geometric phase. These phase factors arise naturally when considering the adiabatic evolution of a state vector in Hilbert space [1–3]. Besides this deeper insight into geometric and topological notions at an experimentally feasible scale, non-Abelian phases (holonomies) are important for holonomic and topological quantum computation, where they offer parametric robustness to increase stability of the computational process [4, 5]. Consequently, there has been increased interest in the study and implementation of artificial gauge fields and symmetry groups [6]. Successful implementations ranged from single artificial gauge fields in photonic [7], superconducting [8], and atomic systems [9] to experimental simulation of lattice gauge theories [10].

In recent years, a novel approach was put forward to realise geometric phases in terms of integrated photonic structures such as laser-written waveguides in fused silica. This has been proven to be a versatile tool box that combines the proven capabilities of modern optics with a high degree of interferometric stability [11]. For instance, the emergence of a non-Abelian Berry phase was observed when injecting coherent states of light into topologically guided modes [12, 13], whereas other implementations made use of a tripod arrangement of evanescently coupled waveguides [14]. In Ref. [15], a proposal based on a photonic bus mode was studied with the view to implement a controlled-NOT gate on single photons. An extension to an  $N$ -pod scheme with arbitrary photon-number states injected was proposed in Ref. [16]. However, all the above-mentioned proposals rely on power-orthogonality of transverse modes. In general, the devi-

ations from mode orthogonality can significantly distort the dynamics of light in coupled-mode systems.

In our present work, we overcome the limitations of the weak-coupling regime by investigating the properties of geometric phases within the framework of nonorthogonal coupled-mode theory (NOCMT). In this setting, the nonorthogonality of transverse modes comes to light when decreasing the separation between adjacent waveguides. In this regime, the energy splitting between an adiabatic subspace and excited states may be large, thus favouring the generation of an adiabatic quantum holonomy. We present an optical setup for the generation of  $U(2)$ -valued and  $U(3)$ -valued geometric phases arising from tripod and tetrapod arrangements of waveguides, respectively, into which coherent light is being injected. After an expansion of the system in terms of normal modes, an analytical computation of the geometric phase reveals that the symmetry of dark states protects the state of light from any distortion.

The article is structured as follows. In Sec. II, we review the nonorthogonal coupled-mode theory (NOCMT) for a network of weak-index contrast waveguides. Sec. III is dedicated to the study of a tripod arrangement of waveguides in an experimentally feasible setting. We compute its geometric phase from a normal mode expansion of the dark states and compare it to a numerical propagation of the longitudinal fields, thus quantifying the diabatic error. In Sec. IV, the influence of higher-order coupling and self-coupling is illuminated using the example of a  $U(3)$ -valued geometric phase generated from an optical tetrapod. Finally, Sec. V contains a summary as well as some concluding remarks.

## II. NONORTHOGONAL COUPLED-MODE THEORY

Since the inception of the concept of coupled modes in electromagnetic systems [17, 18], coupled-mode theory has become a well-established tool in the description of parametric nonlinear devices, waveguide structures, optical fibre networks and various other optoelectronic structures [19–21]. The starting point of our investi-

---

\* stefan.scheel@uni-rostock.de

gation is the propagation of coherent light in a linear, lossless, and isotropic medium patterned with an inhomogeneous lattice of  $N$  waveguides with refractive-index profile  $n(\mathbf{r}) = n_0 + \sum_j \Delta n_j(\mathbf{r})$ , where  $n_0$  is the refractive index of the host material and  $\Delta n_j$  is the refractive-index contrast of the  $j$ th waveguide. The dynamics of an electromagnetic wave is determined by the inhomogeneous wave equation for the electric field  $\mathbf{E}(\mathbf{r}, t)$

$$\nabla^2 \mathbf{E} - \frac{n^2}{c^2} \partial_t^2 \mathbf{E} = \mathbf{E} \cdot \nabla \ln n^2, \quad (1)$$

where  $c$  denotes speed of light in vacuum. Under the assumption of a weak refractive-index contrast, that is  $\nabla \ln n^2 \approx \mathbf{0}$ , Eq. (1) turns into a homogeneous wave equation. It follows that the Helmholtz equation for the paraxial propagation (slowly varying envelope) of an electromagnetic plane wave  $\mathbf{E}(\mathbf{r}, t) = \mathbf{E}(\mathbf{r})e^{i(\omega t - \beta z)}$  reads

$$(\nabla_{\perp}^2 + \lambda^{-2} n^2(\mathbf{r}) - 2i\beta \partial_z - \beta^2) \mathbf{E}(\mathbf{r}) = \mathbf{0} \quad (2)$$

where  $\lambda = c/\omega$ ,  $z$  denotes the propagation coordinate,  $\beta$  is the propagation constant, and  $\nabla_{\perp}^2$  denotes the Laplacian with respect to the transverse coordinates  $\mathbf{r}_{\perp}$ . In a weak index-contrast lattice we have  $\Delta n_j \ll n_0$ , hence the vector character of the Helmholtz equation can be neglected by factoring out a constant unit vector  $\boldsymbol{\nu}$ , because polarization effects at the interface of a waveguide become unimportant, and scalar wave theory can be applied [22]. For the treatment of coupled-mode theory that includes high-index contrast waveguides we refer the reader to Ref. [23].

In the light of the assumption of weak index contrast, we expand the wave packet in terms of tight-binding modes as

$$\mathbf{E}(\mathbf{r}) = \sum_{j=1}^N a_j(z) w_j(\mathbf{r}) \boldsymbol{\nu}, \quad (3)$$

where  $w_j$  is the transverse field mode that is localised around the waveguide  $\Delta n_j$ , and  $a_j$  is the corresponding longitudinal field amplitude determining the dynamics of the light field. The former constitute a quasi-complete (complete for divergence free fields) basis in which fields with compact support over the transverse plane can be expanded. Here we assume that the shape of the transverse field  $w_j$  remains constant throughout the propagation. However, because we consider waveguides that vary their position in the transverse plane along the propagation direction, the fields  $w_j$  depend still on  $z$ . On the other hand, in any typical setup the waveguide position changes only very slowly over the propagation length (paraxial approximation), so that we can safely assume  $w_j(\mathbf{r}) \approx w_j(\mathbf{r}_{\perp})e^{i\beta_j z}$  with an individual propagation constant  $\beta_j$  of the  $j$ th waveguide. The latter ones can be neglected throughout this work by noting that they act merely as offsets when considering an identical writing process for each waveguide.

We assume the transverse fields to satisfy their own Helmholtz equation in the  $(x, y)$ -plane in the absent of the other waveguides, i.e.

$$\left( \nabla_{\perp}^2 + \lambda^{-2} [n_0 + \Delta n_j(\mathbf{r})]^2 - \beta^2 \right) w_j(\mathbf{r}_{\perp}) = 0. \quad (4)$$

This puts the expansion (3) in the light of a weighted eigenmode expansion. We can simplify the above expression by noting that for a weak index contrast we have  $[n_0 + \Delta n_j]^2 \approx n_0^2 + 2n_0 \Delta n_j$  and  $\beta^2 \approx n_0^2/\lambda^2$ . It thus follows that Eq. (4) takes the form

$$\left( \frac{\lambda^2}{2n_0} \nabla_{\perp}^2 + \Delta n_j(\mathbf{r}) \right) w_j(\mathbf{r}_{\perp}) = 0. \quad (5)$$

Inserting the ansatz (3) into Eq. (2), making use of Eq. (5) and employing the same assumptions as before, we obtain

$$\sum_{j=1}^N \left( i\lambda \partial_z a_j w_j - \sum_{\substack{m=1 \\ m \neq j}}^N \Delta n_m a_j w_j \right) = 0. \quad (6)$$

When contracting Eq. (6) with  $w_k^*$ , we observe that the transverse fields overlap with the surrounding waveguides (sites) and their modes gives rise to transverse interactions (see Fig. 1). Here, we distinguish between two

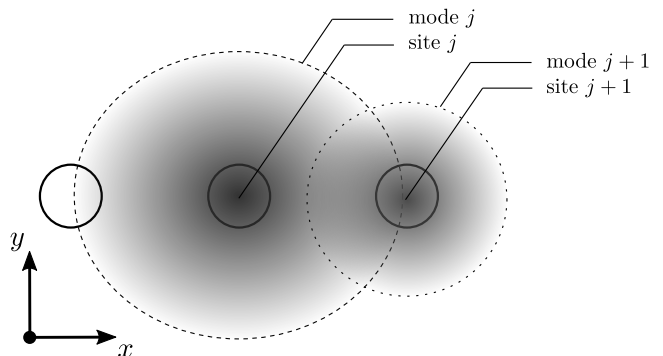


FIG. 1. Schematic front view of evanescently coupled waveguides (black circles). Each site  $j$  supports a fundamental transverse mode  $w_j$  (shaded areas). The modes extend towards the nearest neighbouring sites.

different contributions that occur in Eq. (6) after contraction, namely

$$\begin{aligned} \kappa_{jk} &= \frac{1}{\lambda} \sum_{\substack{m=1 \\ m \neq j}}^N \int_{S_{\infty}} \Delta n_m w_k^* w_j d^2 \mathbf{r}_{\perp}, \\ \sigma_{jk} &= \int_{S_{\infty}} w_k^* w_j d^2 \mathbf{r}_{\perp}, \end{aligned} \quad (7)$$

where we integrate over the entire  $(x, y)$ -plane  $S_{\infty}$ . In Eq. (7),  $\kappa_{jk} \approx \frac{1}{\lambda} \int_{S_{\infty}} \Delta n_k w_k^* w_j d^2 \mathbf{r}_{\perp}$  is the evanescent coupling between waveguides  $j$  and  $k$ , while  $\sigma_{jk}$  describes

the overlap of their respective transverse modes. In particular, there is also a self-coupling  $\nu_j = \kappa_{jj}$  due to the presence of other waveguides around the  $j$ th mode. The latter is usually the smallest contribution to the dynamical propagation (6). This can be seen from Fig. 2 where these quantities were computed for two adjacent (identically written) cylindrical waveguides as a function of their separation. We considered a scenario in which each waveguide supports only its first transverse mode  $w_j(\mathbf{r}_\perp)$ , given in terms of Bessel functions [24]. These assumptions are not too restrictive, as monomode operation and mode synchronism are often required as operating conditions. Furthermore, due to mode overlaps, the transverse modes form a nonorthogonal basis for describing the light propagation. The nonorthogonality can be neglected if the distance between adjacent waveguides is large. Then one works in the regime of OCMT, i.e.  $\sigma_{jk} \approx 0$  for  $j \neq k$  [11, 25, 26].

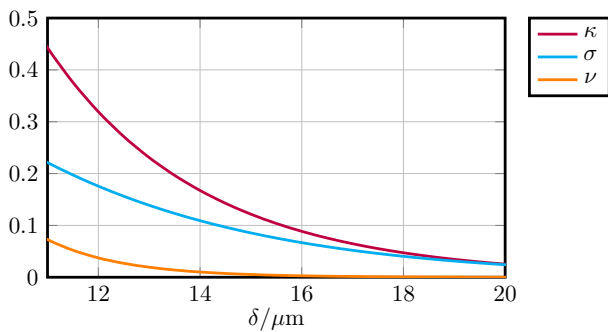


FIG. 2. Coupling  $\kappa$  (in  $\text{mm}^{-1}$ ), overlap  $\sigma$ , and self-coupling  $\nu$  (in  $\text{mm}^{-1}$ ) between two adjacent waveguides as a function of their separation  $\delta$  (measured from the center). The results are shown for cylindrical fibres of radius  $R = 4.8 \mu\text{m}$  with bulk index  $n_0 = 1.452$  and weak contrast  $n_1 = 6.53 \cdot 10^{-4}$  for the inside of each waveguide. The wavelength of the injected light beam considered, is  $\lambda = 633 \text{ nm}$ . The interpolating functions were obtained by evaluating Eq. (7) for several values of  $\delta$ .

With the definitions from Eqs. (7) at hand, the coupled-mode equations become

$$i \sum_{j=1}^N \sigma_{jk} \partial_z a_j = \sum_{j=1}^N \kappa_{jk} a_j. \quad (8)$$

This form of the paraxial Helmholtz equation resembles a discrete Schrödinger equation. Equation (8) can be reformulated as a first-order matrix differential equation in  $z$ , with  $(\mathbf{\Sigma})_{jk} = \sigma_{jk}$  and  $(\mathbf{K})_{jk} = \kappa_{jk}$  being the power and coupling matrix, respectively. Because  $\mathbf{\Sigma}$  and  $\mathbf{K}$  do not commute in general, the generator  $\mathbf{\Sigma}^{-1}\mathbf{K}$  of the dynamics is not necessarily Hermitian, and  $\mathbf{a}^\dagger\mathbf{a}$  would not be conserved throughout the propagation. Particularly, we observe that these generators of the NOCMT lie within the class of real-valued non-symmetric matrices. Nevertheless, the modified intensity distribution  $\mathbf{a}^\dagger\mathbf{\Sigma}\mathbf{a}$  (POVM measurement) remains constant as long as  $\mathbf{K}$  is Hermitian, that is, dissipative effects are negligible as assumed.

The non-Hermitian nature of Eq. (8) can even be lifted completely by transforming to a set of longitudinal normal modes  $\{b_j(z)\}_{j=1}^N$  such that the overall propagation is unitary [25]. Even though we did not start our derivation from power-orthogonal modes, conservation of energy demands that such normal modes always exist. Obviously, in contrast to the waveguide mode  $a_j$ , the corresponding normal mode  $b_j$  will contain contributions from adjacent waveguides. To be precise, their relation is given by the conserved quantity  $\mathbf{b}^\dagger\mathbf{b} = \mathbf{a}^\dagger\mathbf{\Sigma}\mathbf{a}$ . Moreover, because the power matrix  $\mathbf{\Sigma}$  is positive definite, there exists a (non-unique) matrix  $\mathbf{Q}$  such that  $\mathbf{\Sigma} = \mathbf{Q}^\dagger\mathbf{Q}$ . It follows that the normal modes are given by the transformation  $\mathbf{b} = \mathbf{Q}\mathbf{a}$ . With these preparations, Eq. (8) can be rewritten as

$$i\partial_z\mathbf{b} = \mathbf{H}\mathbf{b}, \quad (9)$$

where  $\mathbf{H}$  is given by [25]

$$\mathbf{H} = (\mathbf{Q}^{-1})^\dagger \mathbf{K} \mathbf{Q}^{-1}, \quad (10)$$

which is Hermitian as long as  $\mathbf{K} = \mathbf{K}^\dagger$ . From similarity with Eq. (10) it follows that  $\mathbf{\Sigma}^{-1}\mathbf{K}$  is always diagonalizable with real spectrum.

### A. Adiabatic Propagation

While a general state vector  $\Psi(z)$  evolves according to Eq. (9), under the adiabatic assumption any initial preparation  $\Psi(z_0)$  in a dark subspace (zero-eigenvalue eigenspace) will be mapped to a state  $\Psi(z_f) = \mathbf{U}(z_0, z_f)\Psi(z_0)$  that is also in the dark subspace. Then, we can expand the state  $\Psi$  at every instance  $z$  in terms of the dark states, i.e.  $\Psi(z) = \sum_a U_{ab}(z)\mathbf{d}_a(z)$ , with initial condition  $\Psi(z_0) = \mathbf{d}_a(z_0)$ . Inserting this ansatz into Eq. (9) and following Ref. [3], we obtain  $(\mathbf{U}^{-1}\partial_z\mathbf{U})_{ba} = (\mathbf{A}_z)_{ab}$  where we used  $\mathbf{H}\Psi = \mathbf{0}$  for states  $\Psi$  in the dark subspace. Here we defined the adiabatic connection [27] as  $(\mathbf{A}_z)_{ab} = \mathbf{d}_b^\dagger\partial_z\mathbf{d}_a$ . A formal solution for  $\mathbf{U}$  is then given in terms of the matrix exponential

$$\mathbf{U}(z_0, z_f) = \mathcal{T} \exp \int_{z_0}^{z_f} \mathbf{A}_z dz, \quad (11)$$

where  $\mathcal{T}$  denotes  $z$ -ordering.

For a collection of coupled waveguides, the  $z$ -dependence of the system is functionally connected to the distances between the waveguides  $\{\delta_\mu(z)\}_\mu$  that form local coordinates of an abstract parameter space  $\mathcal{M}$  (control manifold). Then, the propagation along the  $z$ -direction can equivalently be viewed as a parameter variation along a curve  $\mathcal{C} : [z_0, z_f] \rightarrow \mathcal{M}$ . In the following sections we are not interested in arbitrary paths, but only those that (approximately) form loops in  $\mathcal{M}$ , i.e.  $\mathcal{C}(z_0) = \mathcal{C}(z_f)$ . Population transfer between waveguides associated with such a loop appears to be robust against stochastic fluctuations of the control parameter, as the transformation  $\mathbf{U}(z_0, z_f)$  only depends on the area enclosed by the loop  $\mathcal{C}$  [28].

### III. TRIPOD ARRANGEMENT OF WAVEGUIDES

In order to examine the properties of geometric phases in relation to nonorthogonal modes more closely, we shall focus on a benchmark example that can be implemented using the current state of technology. A schematic representation of the waveguide network under investigation is shown in Fig. 3. There, the outer waveguides L, R, and U interact only implicitly via the central waveguide C (nearest-neighbour coupling). To be more precise, we consider a situation in which the transverse fields of the outer waveguides have couplings and overlaps that can be safely disregarded. Then, the coupling matrix of the system is

$$\mathbf{K} = \sum_{j \neq C} \kappa_{jC} \left( \mathbf{w}_j^\dagger \mathbf{w}_C + \mathbf{w}_C^\dagger \mathbf{w}_j \right) + \sum_j \nu_j \mathbf{w}_j^\dagger \mathbf{w}_j,$$

where  $j$  enumerates the waveguides  $\{L, R, U, C\}$ . Here,  $\{\mathbf{w}_j\}_j$  denotes the standard basis in  $\mathbb{C}^4$  that forms an orthonormal representation of the transverse eigenmodes of the  $j$ th waveguide. For the moment, we neglect self-coupling on the matrix diagonal, as it appears to be the smallest contribution to the overall propagation. The corresponding power matrix of the system then reads

$$\mathbf{\Sigma} = \sum_{j \neq C} \sigma_{jC} \left( \mathbf{w}_j^\dagger \mathbf{w}_C + \mathbf{w}_C^\dagger \mathbf{w}_j \right) + \sum_j \mathbf{w}_j^\dagger \mathbf{w}_j, \quad (12)$$

where we assumed normalised transverse modes such that  $\sigma_{jj} = 1$ . The setup depicted in Fig. 3 is known as a tripod system. The tripod scheme, arising in different physical settings, is often used as a starting point for the generation of  $U(2)$ -valued phases, see, e.g., Refs. [29–31].

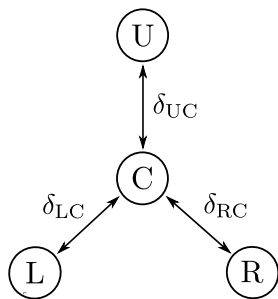


FIG. 3. Front view of the tripod arrangement, arrows indicate interactions between the outer waveguides and the central waveguide. Within NOCMT, this includes evanescent coupling as well as the overlap of transverse modes. In OCMT, this overlap is neglected. The interaction strength depends on the separation  $\delta_{iC}$  between the corresponding waveguides.

One possible transformation between waveguide and normal modes can be obtained by a Cholesky factorisation of the matrix (12), that reads

$$\mathbf{Q} = \sum_{j \neq C} \left( \sigma_{jC} \mathbf{w}_j^\dagger \mathbf{w}_C + \mathbf{w}_j^\dagger \mathbf{w}_j \right) + \sqrt{1 - \sigma^2} \mathbf{w}_C^\dagger \mathbf{w}_C, \quad (13)$$

where we introduced the vector  $\boldsymbol{\sigma} = (\sigma_{LC}, \sigma_{RC}, \sigma_{UC})$ . From the matrix (13) we can compute the Hermitian generator for the evolution of normal modes according to Eq. (10), and we find

$$\mathbf{H} = \sum_{j \neq C} s \kappa_{jC} \left( \mathbf{w}_j^\dagger \mathbf{w}_C + \mathbf{w}_C^\dagger \mathbf{w}_j \right) - 2s^2 \boldsymbol{\sigma} \cdot \boldsymbol{\kappa} \mathbf{w}_C^\dagger \mathbf{w}_C,$$

with  $\boldsymbol{\kappa} = (\kappa_{LC}, \kappa_{RC}, \kappa_{UC})$  and  $s = 1/\sqrt{1 - \sigma^2}$ . The system's dark states

$$\begin{aligned} \mathbf{d}_1 &= \sin \theta \mathbf{w}_L - \cos \theta \mathbf{w}_R, \\ \mathbf{d}_2 &= \cos \theta \sin \varphi \mathbf{w}_L + \sin \theta \sin \varphi \mathbf{w}_R - \cos \varphi \mathbf{w}_U, \end{aligned} \quad (14)$$

satisfy  $\mathbf{H} \mathbf{d}_a = \mathbf{0}$ , where we defined  $\theta = \arctan(\kappa_{RC}/\kappa_{LC})$  and  $\varphi = \arctan(\kappa_{UC}/\sqrt{\kappa_{LC}^2 + \kappa_{RC}^2})$ . Quite remarkably, as long as the second-order (next-nearest-neighbour) contributions to the coupling [32] as well as self-coupling are negligible, the introduction of mode overlaps does not break the degeneracy of the system, and still gives rise to a two-fold degenerate dark subspace similar to its counterpart in OCMT [14]. In particular, the dark states of  $\mathbf{H}$  have the same structure as the ones found in OCMT but with their coefficients now giving the population of the associated normal mode that differ from the individual modes of each waveguide.

With the dark states known, computing the connection  $\mathbf{A}_z$  becomes a straightforward task and, thus, the matrix exponential (11) can be evaluated analytically to

$$\mathbf{U}(z_0, z_f) = \begin{pmatrix} \cos \phi & \sin \phi \\ -\sin \phi & \cos \phi \end{pmatrix}, \quad (15)$$

written in the basis  $\{\mathbf{d}_a(z)\}_a$ . Here

$$\phi(z_0, z_f) = \int_{z_0}^{z_f} \frac{\kappa_{UC} (\kappa_{LC} \partial_z \kappa_{RC} - \kappa_{RC} \partial_z \kappa_{LC})}{\sqrt{\kappa_{LC}^2 + \kappa_{RC}^2 + \kappa_{UC}^2} (\kappa_{LC}^2 + \kappa_{RC}^2)} dz \quad (16)$$

is a phase factor depending only on the geometry of the associated parameter variation  $\mathcal{C}$ . The holonomy matrix (15) is the same unitary transformation as for the case of orthogonal transverse modes [14]. This implies that the results of the NOCMT and the OCMT predict the same output state as long as the evolution takes place solely in the dark subspace. This means that the geometric phase generated from the tripod is robust against the nonorthogonal nature of transverse modes. This is a remarkable result as, in general, the deviations from mode-orthogonality can significantly distort the dynamics of light in a coupled-mode system.

#### A. Propagation with Gaussian-shaped geometries

Here, we present an experimentally feasible parameter loop  $\mathcal{C}$  that can be realised by current laser-writing

techniques [11]. Suppose one implements the geometry

$$\begin{aligned}\delta_{\text{LC}}(z) &= \Delta - \Omega \exp\left(-\frac{(z - \bar{z} - \tau)^2}{T^2}\right), \\ \delta_{\text{RC}}(z) &= \Delta - \Omega \exp\left(-\frac{(z - \bar{z} + \tau)^2}{T^2}\right), \\ \delta_{\text{UC}}(z) &= \Delta_U,\end{aligned}\quad (17)$$

in which the central waveguide is assumed to remain at the origin of the transverse plane, while the separation to the L and R waveguide changes according to a Gaussian function. In Eq. (17),  $\bar{z}$  denotes half the total propagation length,  $\Delta - \Omega$  is the minimal separation between waveguide L (R) and the central waveguide C, with waveguide U having constant distance  $\Delta_U$ . Furthermore,  $T$  is the width parameter, and  $\tau$  is the separation of the two Gaussian peaks from the center at  $\bar{z}$ . The relevant coupling strengths and overlaps of the respective waveguides can be determined from their mutual separation, shown in Fig. 2. Given the variation (17), the respective coupling constants and overlaps are shown in Fig. 4.

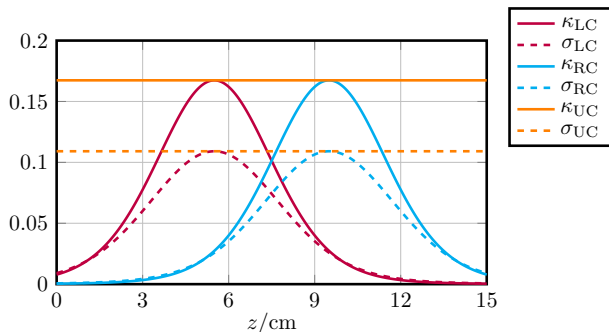


FIG. 4. Couplings  $\kappa_{iC}$  (in  $\text{mm}^{-1}$ ) and overlaps  $\sigma_{iC}$  between the  $i$ th outer waveguide and the central waveguide as a function of the propagation distance  $z$  for the case of the  $z$ -dependent waveguide position (17). The chosen parameters are  $\Delta = 40 \mu\text{m}$ ,  $\Delta_U = 14 \mu\text{m}$ ,  $\Omega = 26 \mu\text{m}$ ,  $T = 8 \text{cm}$ , and  $\tau = 2 \text{cm}$ .

A parameter loop starting at the initial point  $\delta_0 = (\Delta, \Delta, \Delta_U)$  will induce a nontrivial mixing of states

$$\mathbf{d}_1(\delta_0) \approx \mathbf{w}_L, \quad \mathbf{d}_2(\delta_0) \approx \mathbf{w}_R.$$

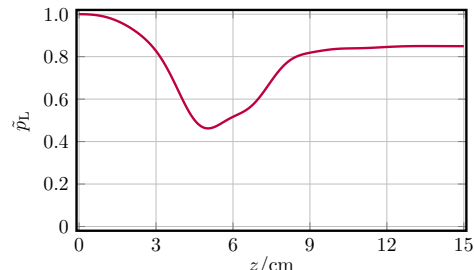
After integration of the phase factor (16) and subsequent evaluation of the transformation (15), this mixing can be given explicitly. The adiabatic limit is applicable if the loop  $\mathcal{C}$  given by Eq. (17) is traversed slowly enough compared to the energy splitting between the dark subspace and the excited bright subspaces. We found that the separation between dark and bright states is slightly shifted when compared to the eigenvalue splitting known from OCMT, due to the contribution from mode overlaps. In order to evaluate to which extent the adiabatic approximation is justified in NOCMT, we compute the

(expected) gate fidelity  $0 \leq \bar{F} \leq 1$  in terms of input state fidelities

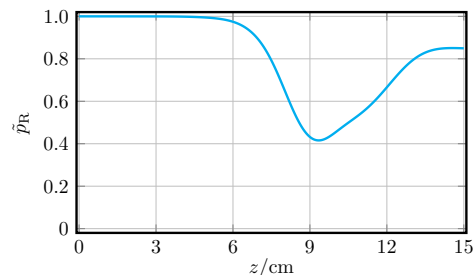
$$F_{\Psi(z_0)} = |\tilde{\Psi}(z_f)^\dagger \mathbf{Q}^{-1}(z_f) \mathbf{U}(z_f) \Psi(z_0)|^2, \quad (18)$$

with  $\mathbf{U}(z_f) \Psi(z_0)$  being the ideal output state predicted by the holonomic theory (15) and  $\tilde{\Psi}(z_f)$  obtained from a numerical propagation subject to the paraxial Helmholtz equation (8). For the scenario under study, the gate fidelity of the dark state ensemble  $\{\{1/2, \mathbf{w}_L\}, \{1/2, \mathbf{w}_R\}\}$  amounts to approximately  $\bar{F} \approx 98.6\%$ .

We can conclude that robust adiabatic parallel transport of an initial wave packet can be achieved within the range of experimentally feasible setups, despite the influence of mode-nonorthogonality. In fact, the expected distortion from close-coupling dynamics comes to light when one of the bright states  $\mathbf{w}_U$  or  $\mathbf{w}_C$  is excited. In Fig. 5 we compare the population transfer between the waveguides for different initial input states. One can clearly see the robustness of the dark states, while the excited states are exposed to more rapid population transfer. In fact, when adding the bright states to the input ensemble, a gate error emerges that is not of diabatic nature, but has its origin in the fact that the parameter variation (17) does not form a perfect loop. This matching error of input and output basis is rather small for the dark states but gets amplified for the bright states due to rapid intensity oscillations, thus leading to a substantial decrease in gate fidelity,  $\bar{F} \approx 88.9\%$ . The relation between mode-nonorthogonality and rapid intensity oscillations was experimentally verified in Ref. [33]. In general, the robustness of dark states can be attributed to their form given by Eq. (14) which is independent of  $\sigma_{iC}$  and therefore identical to their counterparts in OCMT [14]. Hence, despite the overlaps, absence of light in waveguide C can still be used as a measure of adiabaticity.



(a) Intensity in site L for  $\Psi(z_0) = \mathbf{w}_L$ .



(b) Intensity in site R for  $\Psi(z_0) = \mathbf{w}_R$ .

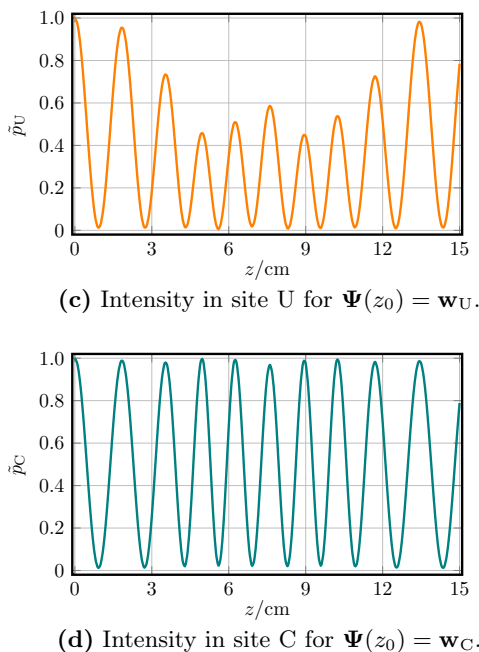


FIG. 5. Simulated propagation of  $\Psi(z)$  in term of waveguide modes [subject to Eq. (8)] for the waveguide position (17) under investigation. The four plots show the change of intensity throughout propagation for different initial input states  $\{\mathbf{w}_j\}_j$ . It can be seen that the bright states (U and C) are subject to rapid intensity fluctuations due to deviations from mode orthogonality. The parameter values are  $\Delta = 40 \mu\text{m}$ ,  $\Delta_U = 14 \mu\text{m}$ ,  $\Omega = 26 \mu\text{m}$ ,  $T = 8 \text{ cm}$ , and  $\tau = 2 \text{ cm}$ .

#### IV. HIGHER-ORDER COUPLING IN THE TETRAPOD ARRANGEMENT

We now turn to the influence of self-coupling and higher-order contributions in a waveguide network which had been neglected in our calculations thus far. These effects potentially break the degeneracy structure of the system under investigation. We found numerically that, in the tripod arrangement, these contributions are completely negligible for the propagation lengths investigated ( $|z_f - z_0| \leq 15 \text{ cm}$ ). However, this result depends crucially on the distance behaviour shown in Fig. 2, and does not need to be valid beyond step-index waveguides.

In order to show that coupling beyond nearest-neighbour hopping as well as self-coupling can become relevant when the distance between waveguides is substantially decreased, we now turn to a tetrapod arrangement depicted in Fig. 6. Placing more waveguides around the central site will inevitably result in a system having no degeneracy at all. The coupling and power matrices of the (ideal) tetrapod system without self-coupling and higher-order effects are given by

$$\mathbf{K} = \sum_{j \neq C} \kappa_{jC} \left( \mathbf{w}_j^\dagger \mathbf{w}_C + \mathbf{w}_C^\dagger \mathbf{w}_j \right) \quad (19)$$

and

$$\Sigma = \sum_{j \neq C} \sigma_{jC} \left( \mathbf{w}_j^\dagger \mathbf{w}_C + \mathbf{w}_C^\dagger \mathbf{w}_j \right) + \sum_j \mathbf{w}_j^\dagger \mathbf{w}_j, \quad (20)$$

where  $j$  runs through the alphabet  $\{N, E, S, W, C\}$ , and hence  $\{\mathbf{w}_j\}_j$  might be thought of as the standard basis in  $\mathbb{C}^5$ . For this system, the adiabatic propagation of normal modes will generate a  $U(3)$ -valued mixing within the three-fold degenerate dark subspace.

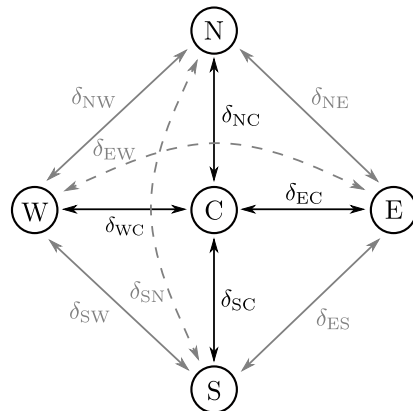


FIG. 6. Front view of the tetrapod arrangement, arrows indicate interaction between the respective waveguides. Within the NOCMT this includes evanescent coupling as well as the overlap of transverse modes. In the case of OCMT the overlap is neglected. The strength of interaction depends on the separation  $\delta_{iC}$  between the corresponding waveguides. Black arrows were chosen for nearest-neighbour coupling (first order). Grey solid lines are reserved for next-nearest neighbour coupling (second order), while grey dotted lines depict coupling between opposite placed waveguides (third order).

Higher-order coupling becomes relevant as soon as the propagation length of the evolution is substantially increased. In this regime, we can assume adiabaticity to apply. Then, the matrices in Eq. (19) and Eq. (20) are no longer sparse, but have only nonvanishing entries. The diagonal entries of  $\mathbf{K}$  now contain the self-couplings  $\nu_j$ . In the following, we will study the influence of such contributions on a benchmark geometry

$$\begin{aligned} \delta_{NC}(z) &= \Delta - \Omega \exp\left(-\frac{(z - \bar{z} - \tau)^2}{T^2}\right), \\ \delta_{EC}(z) &= \Delta - \Omega \exp\left(-\frac{(z - \bar{z})^2}{T^2}\right), \\ \delta_{SC}(z) &= \Delta - \Omega \exp\left(-\frac{(z - \bar{z} + \tau)^2}{T^2}\right), \\ \delta_{WC}(z) &= \Delta_W. \end{aligned} \quad (21)$$

In the chosen waveguide geometry, the evolution of coherent light approximately starts and ends at the point



$\delta_0 = (\Delta, \Delta, \Delta, \Delta_W)$ , where the holonomy will generate a mixing of dark states

$$\mathbf{d}_1(\delta_0) \approx \mathbf{w}_N, \quad \mathbf{d}_2(\delta_0) \approx \mathbf{w}_E, \quad \mathbf{d}_3(\delta_0) \approx \mathbf{w}_S.$$

Given the geometry (21), we can derive the  $z$ -dependent form of the relevant parameters from Fig. 2. Knowing these parameters allows us, by simple geometric considerations (cf. Fig. 6), to construct higher-order couplings and overlaps as well. In Fig. 7, the coupling strengths of these different contributions is shown for the waveguide N. One observes clearly how the higher-order couplings have a substantially smaller influence compared to the nearest-neighbour coupling. Nevertheless, for longer propagation lengths (e.g.  $|z_f - z_0| = 40$  cm) these contributions will lead to a deviation in the intensity distribution from the evolution predicted by the propagation through the ideal tetrapod system.

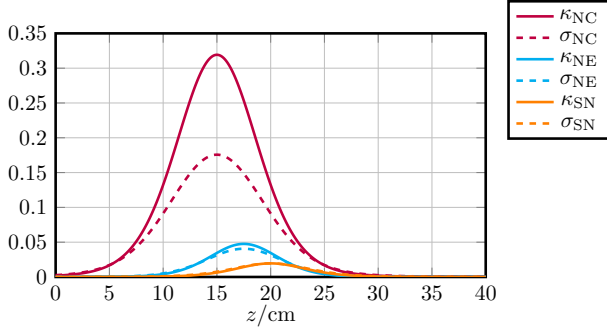


FIG. 7. Couplings (in  $\text{mm}^{-1}$ ) and overlaps between the northern (N) waveguide and  $j$ th waveguide ( $j \in \{C, E, S\}$ ) of the tetrapod arrangement as a function of the propagation distance  $z$  for the waveguide geometry (21). Coupling to the central (C) waveguide is of first order, coupling to the eastern (E) waveguide is of second order, and coupling to the south (S) waveguide is of third order. The relevant parameters are given by  $\Delta = 38 \mu\text{m}$ ,  $\Delta_W = 12 \mu\text{m}$ ,  $\Omega = 26 \mu\text{m}$ ,  $T = 15$  cm, and  $\tau = 5$  cm.

We also investigated the change of self-coupling  $\nu_j(z)$  of each respective waveguide. There we observed that the order of magnitude of the self-coupling in the outer waveguides lies between those of the second-order and third-order contributions. However, the self-coupling  $\nu_C$  is substantially larger, as the central waveguide mode is closely surrounded by the other waveguides.

In Fig. 8, the propagation through the ideal tetrapod (solid line) is compared to a propagation including higher-order couplings and self-coupling (dashed line). The state was propagated numerically for an initial input  $\mathbf{w}_N$ . Our results show that these additional effects (mostly second-order coupling and self-coupling  $\nu_C$ ) lead to increased population transfer between the waveguides. Due to symmetry-breaking, this additional population transfer will not be robust against parametric fluctuations and mode-nonorthogonalities as it is no longer described by a parallel transport in the degenerate dark subspace of the tetrapod.

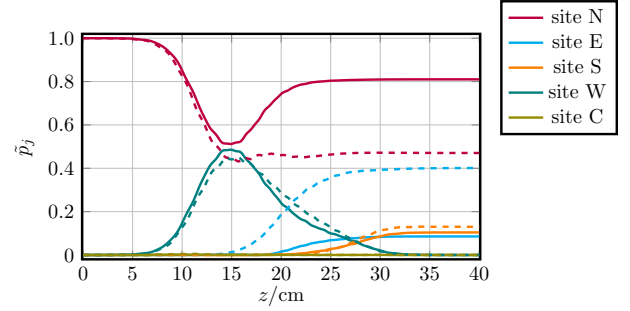


FIG. 8. Intensity distribution for the tetrapod arrangement subject to the geometry (21). The solid lines belong to the ideal tetrapod [Eq. (19) and Eq. (20)], while the dashed lines describe propagation including higher-order couplings as well as self-coupling. The results were computed via a numerical simulation of Eq. (8) for an initial wave package  $\mathbf{w}_N$ , with parameters  $\Delta = 38 \mu\text{m}$ ,  $\Delta_W = 12 \mu\text{m}$ ,  $\Omega = 26 \mu\text{m}$ ,  $T = 15$  cm, and  $\tau = 5$  cm for a network of 40 cm total length.

## V. CONCLUSION

In this article, we have shown that the generation of geometric phases in integrated photonic waveguide structures can be considered within the framework of nonorthogonal coupled-mode theory. General arguments show that, including the nonorthogonality of transverse modes leads to a set of tight-binding equations governing an evolution in which the conventional intensity distribution is not necessarily conserved. This issue was lifted by means of a normal mode expansion. An analytical computation of the geometric phase and a subsequent evaluation of the intensity distribution for the tripod system showed a robustness of the adiabatic parallel transport against deviations from mode-orthogonalities as long as adiabaticity holds and higher-order couplings are negligible. A subsequent study of the tetrapod arrangement showed that higher-order coupling as well as self-coupling can become relevant for longer propagation lengths, eventually breaking the degeneracy of the system, thus perturbing the generation of a  $U(3)$ -valued geometric phase. However, for appropriate propagation lengths our numerical simulations of the population transfer between the waveguides showed that high fidelity transformations can be generated when working in the close-coupling regime.

Our work paves the way for the study of adiabatic parallel transport by photonic structures within the close-coupling regime. The symmetry of the dark subspace leads to an inherent robustness of geometric phases towards the distortion of light by mode-nonorthogonalities. Together with their parametric stability, geometric phases can be considered a powerful tool for the generation of stable population transfer of light even within the realm of the nonorthogonal coupled-mode theory.

## ACKNOWLEDGMENTS

Financial support by the Deutsche Forschungsgemeinschaft (DFG SCHE 612/6-1) is gratefully acknowledged.

- 
- [1] Y. Aharonov and D. Bohm, Significance of Electromagnetic Potentials in the Quantum Theory, *Phys. Rev.* **115**, 485 (1959).
- [2] M. V. Berry, Quantal Phase Factors Accompanying Adiabatic Changes, *Proc. R. Soc. London, Ser. A* **392**, 45 (1984).
- [3] F. Wilczek and A. Zee, Appearance of Gauge Structure in Simple Dynamical Systems, *Phys. Rev. Lett.* **52**, 2111 (1984).
- [4] P. Zanardi and M. Rasetti, Holonomic Quantum Computation, *Phys. Lett. A* **264**, 94 (1999).
- [5] J. K. Pachos, *Introduction to Topological Quantum Computation* (Cambridge, Cambridge University Press, 2012).
- [6] M. C. Bañuls, R. Blatt, J. Catani, A. Celi, J. I. Cirac, M. Dalmonte, L. Fallani, K. Jansen, M. Lewenstein, S. Montangero *et al.*, Simulating lattice gauge theories within quantum technologies, *Eur. Phys. J. D* **74**, 165 (2020).
- [7] Y. Lumer, M. A. Bandres, M. Heinrich, L. J. Maczewsky, H. Herzig-Sheinfux, A. Szameit, and M. Segev, Light guiding by artificial gauge fields, *Nat. Photon.* **13**, 339 (2019).
- [8] A. A. Abdumalikov, Jr., J. M. Fink, K. Juliusson, M. Pechal, S. Berger, A. Wallraff, and S. Filipp, Experimental realization of non-Abelian non-adiabatic geometric gates, *Nature (London)* **496**, 482 (2013).
- [9] V. Galitski, G. Juzeliūnas, and I. B. Spielman, Artificial gauge fields with ultracold atoms, *Phys. Today* **72**, 38 (2019).
- [10] E. A. Martinez, C. A. Muschik, P. Schindler, D. Nigg, A. Erhard, M. Heyl, P. Hauke, M. Dalmonte, T. Monz, P. Zoller *et al.*, Real-time dynamics of lattice gauge theories with a few-qubit quantum computer, *Nature (London)* **534**, 516 (2016).
- [11] A. Szameit and S. Nolte, Discrete optics in femtosecond-laser-written photonic structures, *J. Phys. B: At. Mol. Opt. Phys.* **43**, 163001 (2010).
- [12] T. Iadecola, T. Schuster, and C. Chamon, Non-Abelian Braiding of Light, *Phys. Rev. Lett.* **117**, 073901 (2016).
- [13] J. Noh, T. Schuster, T. Iadecola, S. Huang, M. Wang, K. P. Chen, C. Chamon, and M. C. Rechtsman, *Nature Physics (London)* **16**, 989 (2020).
- [14] M. Kremer, L. Teuber, A. Szameit, and S. Scheel, Optimal design strategy for non-Abelian geometric phases using Abelian gauge fields based on quantum metric, *Phys. Rev. Res.* **1**, 033117 (2019).
- [15] A. P. Hope, T. G. Nguyen, A. Mitchell, and A. D. Green-tree, Adiabatic two-photon quantum gate operations using a long-range photonic bus, *J. Phys. B: At. Mol. Opt. Phys.* **48**, 055503 (2015).
- [16] J. Pinske, L. Teuber, and S. Scheel, Highly degenerate photonic waveguide structures for holonomic computation, *Phys. Rev. A* **101**, 062314 (2020).
- [17] J. R. Pierce, *J. Appl. Phys.* **25**, 179 (1954).
- [18] S. A. Schelkunoff, Conversion of Maxwell's Equations into Generalized Telegraphist's Equations, *Bell Syst. Tech. J.* **34**, 995 (1955).
- [19] W. Streifer, M. Osinski, and A. Hardy, Reformulation of the coupled-mode theory of multiwaveguide systems, *J. Lightwave Tech.* **5**, 1 (1987).
- [20] S.-L. Chuang, A coupled mode formulation by reciprocity and a variational principle, *J. Lightwave Tech.* **5**, 5 (1987).
- [21] R. G. Peall and R. R. A. Syms, Comparison between strong coupling theory and experiment for three-arm directional couplers in Ti: LiNbO<sub>3</sub>, *J. Lightwave Tech.* **7**, 540 (1989).
- [22] D. Gloge, Weakly Guiding Fibers, *Appl. Opt.* **10**, 2252, (1971).
- [23] G. Bellanca, P. Orlandi, and P. Bassi, *J. Opt. Soc. Am. A* **35**, 577 (2018).
- [24] B. E. A. Saleh and M. C. Teich, *Fundamentals of Photonics* (New York, Wiley-VCH, 2007).
- [25] H. A. Haus, W. P. Huang, S. Kawakami, and N. A. Whitaker, *J. Lightwave Tech.* **5**, 13 (1987).
- [26] H. A. Haus and W. Huang, Coupled-mode theory, *Proc. IEEE*, **19**, 10 (1991).
- [27] R. Bott and S. S. Chern, Hermitian vector bundles and the equidistribution of the zeros of their holomorphic sections, *Acta Math.* **114**, 71 (1968).
- [28] J. K. Pachos and P. Zanardi, Quantum Holonomies for Quantum Computing, *Int. J. Mod. Phys. B* **15**, 1257 (2001).
- [29] R. G. Unanyan, B. W. Shore, and K. Bergmann, Laser-driven population transfer in four-level atoms: Consequences of non-Abelian geometrical adiabatic phase factors, *Phys. Rev. A* **59**, 2910 (1999).
- [30] A. Recati, T. Calarco, P. Zanardi, J. I. Cirac, and P. Zoller, Holonomic quantum computation with neutral atoms, *Phys. Rev. A* **66**, 032309 (2002).
- [31] L. M. Duan, J. Cirac, and P. Zoller, Geometric Manipulation of Trapped Ions for Quantum Computation, *Science* **292**, 1695 (2001).
- [32] R. Keil, B. Pressl, R. Heilmann, M. Gräfe, G. Weihs, and A. Szameit, Direct measurement of second-order coupling in a waveguide lattice, *Appl. Phys. Lett.* **107**, 241104 (2015).
- [33] S. Weimann, PhD Thesis, *Complex lattice modes in waveguide networks and photonic solids* (University of Rostock, Germany, 2018).